Journal of Materials Chemistry A

COMMUNICATION

Published on 22 June 2026

Cite this: DOI: 10.1039/d5ta10419j

Received 22nd December 2025
Accepted 22nd June 2026

DOI: 10.1039/d5ta10419j

rsc.li/materials-a

Facile design of hydrazone-based Spiro-OMeTAD-alternative hole-transporting material for perovskite solar cells

Aistė Jegorovė,[a] Xiao-Xin Gao,*[c] Povilas Luizys,[a] Maryte Daskeviciene,[a] Shiyu Xing,[c] Riccardo Pau,[c] Julius Petrulevičius,[a] Vygintas Jankauskas,[b] Kasparas Rakstys,[a] Mohammad Khaja Nazeeruddin*[cd] and Vytautas Getautis*[a]

A hydrazone-based hole-transporting material, 9,9′-(hydrazine-1,2-diylidene)bis(N^2,N^2,N^7,N^7-tetrakis(4-methoxyphenyl)-9*H*-fluorene-2,7-diamine) (**V1375**), has been synthesized using a straightforward two-step procedure from commercially available and inexpensive starting reagents, mimicking the synthetically challenging 9,9′-spirobifluorene moiety of well-studied Spiro-OMeTAD. The evaluated thermal properties reveal that pristine **V1375** exhibits a glass transition temperature of 132 °C and high thermal stability, with 5% mass loss occurring at 395 °C. Meanwhile, the measured intrinsic hole-transporting mobility and conductivity reach 2.5×10^{-6} cm^2 V^{-1} s^{-1} and 1.6×10^{-4} S m^{-1}, respectively. A power conversion efficiency of over 24% with improved stability has been achieved by employing the doped **V1375** as a novel HTM in perovskite solar cells, outperforming state-of-the-art Spiro-OMe-TAD.

Introduction

Today, environmental pollution is one of the world's biggest problems, causing ecological issues such as the greenhouse effect, droughts, and floods, and increasing the suffering caused by more frequent and severe hurricanes and heat waves. These disasters lead to food and water shortages, disrupt the global food chain, and threaten biodiversity. Environmental contamination is primarily the result of the usage of non-renewable energy resources, such as oil or coal; therefore, the utilization of clean and renewable energy sources is crucial. Over the past decade, renewable energy sources, such as solar, wind, and geothermal power, have achieved prominence, with their share of global energy generation now exceeding 10%.

[a]*Department of Organic Chemistry, Kaunas University of Technology, Radvilėnų pl. 19, Kaunas, 50254, Lithuania. E-mail: vytautas.getautis@ktu.lt*

[b]*Institute of Chemical Physics, Vilnius University, Saulėtekio al. 3, Vilnius 10257, Lithuania*

[c]*Institute of Chemical Sciences and Engineering, École Polytechnique Fédérale de Lausanne (EPFL), CH 1015, Lausanne, Switzerland. E-mail: xiaoxin.gao@epfl.ch; mdkhaja.nazeeruddin@epfl.ch*

[d]*Department of Mechanical and Energy Engineering, College of Engineering, Imam Abdulrahman Bin Faisal University, P.O. Box 1982, 34212, Dammam, Saudi Arabia*

Solar energy is one of the largest and most accessible energy sources available to humanity, leading to the invention of solar cells. Since 1954,[1] solar technology has evolved significantly, resulting in the development of various types of solar cells. In 2009,[2] the first publication on perovskite solar cells (PSCs) was released, sparking interest among scientists. Since then, intensive research has led to impressive improvements in efficiency, with the highest recorded performance reaching 27%.[3]

Perovskite material is particularly attractive for solar cell applications because of its long carrier diffusion length,[4] high absorption coefficient,[5] low exciton binding energy,[6] high charge carrier mobility,[7] and versatility in layer coating techniques.[8] However, several issues hinder the commercialization of PSCs, including the poor stability of perovskite material[9] and the high cost of commonly used hole-transporting materials (HTMs). Consequently, optimization of synthesis processes is required for developing cost-effective and stable devices.

Although PSCs can generate electricity without a hole-transporting layer (HTL),[10–12] their efficiencies are typically higher when molecular organic HTMs are incorporated into an n–i–p device structure. The highest performances have been achieved using 2,2′,7,7′-tetrakis(*N*,*N*-di-*p*-methoxyphenylamine)-9,9′-spirobifluorene (Spiro-OMeTAD). However, the multi-step synthesis of Spiro-OMeTAD is excessively expensive, as it involves reaction steps that require low temperature (−78 °C), sensitive (*n*-butyllithium or Grignard) reagents and aggressive (Br_2) reagents. In addition, high-purity sublimation-grade Spiro-OMeTAD is required to obtain high-performance devices. Even after optimization of the synthesis, this material still requires four synthesis steps.[13]

For this reason, scientists have focused their attention on developing new HTMs that can be synthesized through simple methods while exhibiting desirable properties. Consequently, numerous new materials, including compounds of spirobifluorene,[14–16] fluorene,[17–19] fluorenylidene,[20–22] and carbazole,[23–25] have been proposed as HTMs for efficient device fabrication. Meanwhile, hydrazones, a well-known and easily

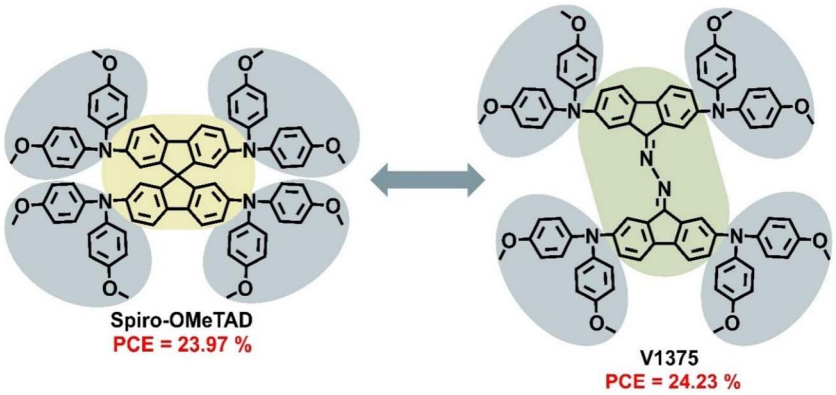

Fig. 1 Chemical structures of Spiro-OMeTAD and hydrazone-based **V1375**.

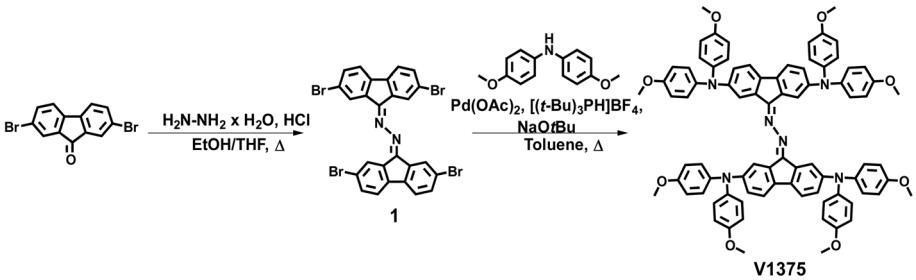

Scheme 1 Synthetic route to intermediate **1** and target compound **V1375**.

synthesised class of materials, have not been widely explored as hole-transporting materials in PSCs. However, over the past decade, they have been among the most popular families of materials used for electrophotographic photoreceptors.[26–28] To the best of our knowledge, only a few studies have investigated the application of hydrazones as HTMs for perovskite solar cells.[29–32]

In this study, we describe a hydrazone-based material, **V1375**, which was synthesized *via* a simple two-step synthesis strategy and used in an n–i–p device configuration (Fig. 1). The power conversion efficiency of perovskite solar cells using **V1375** reaches 24.23%, which is very similar to that achieved with Spiro-OMeTAD (23.97%). Moreover, the long-term stability of the champion solar cell was greater than that of devices using Spiro-OMeTAD.

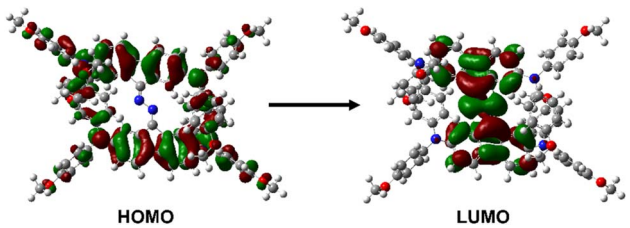

Fig. 2 Frontier Kohn–Sham molecular orbitals of **V1375** were obtained from theoretical calculations at the B3LYP/6-31G(d,p) level of theory.

Results and discussion

Hydrazone-based HTM was synthesized using Buchwald–Hartwig reaction conditions using 4,4′-dimethoxydiphenylamine as a side fragment. As shown in Scheme 1, in the first step, the corresponding central hydrazone-bridged bifluorene fragment

Table 1 Thermal, optical and photophysical properties of **V1375** and Spiro-OMeTAD

HTM	T_g[a] [°C]	T_m[a] [°C]	T_{d5}[a] [°C]	λ_{abs}[b] [nm]	I_P[c] [eV]	μ_0[d] [cm^2 V^{-1} s^{-1}]	σ [S m^{-1}]
V1375	132	303	395	297, 339, 383, 544	4.92	2.5×10^{-6}	1.6×10^{-4}
Spiro-OMeTAD	138	249	413	237, 303, 367, 387	4.91	1.4×10^{-5}	6.4×10^{-5}

[a] Glass transition (T_g), melting point (T_m) and 5% weight loss (T_{d5}) temperatures observed from DSC and TGA measurements, respectively (10 °C min^{-1}, N_2 atmosphere). [b] UV-vis spectra measured in tetrahydrofuran (THF) solution (10^{-4} M). [c] Ionization energies of the films measured using PESA. [d] Mobility value at zero field strength.

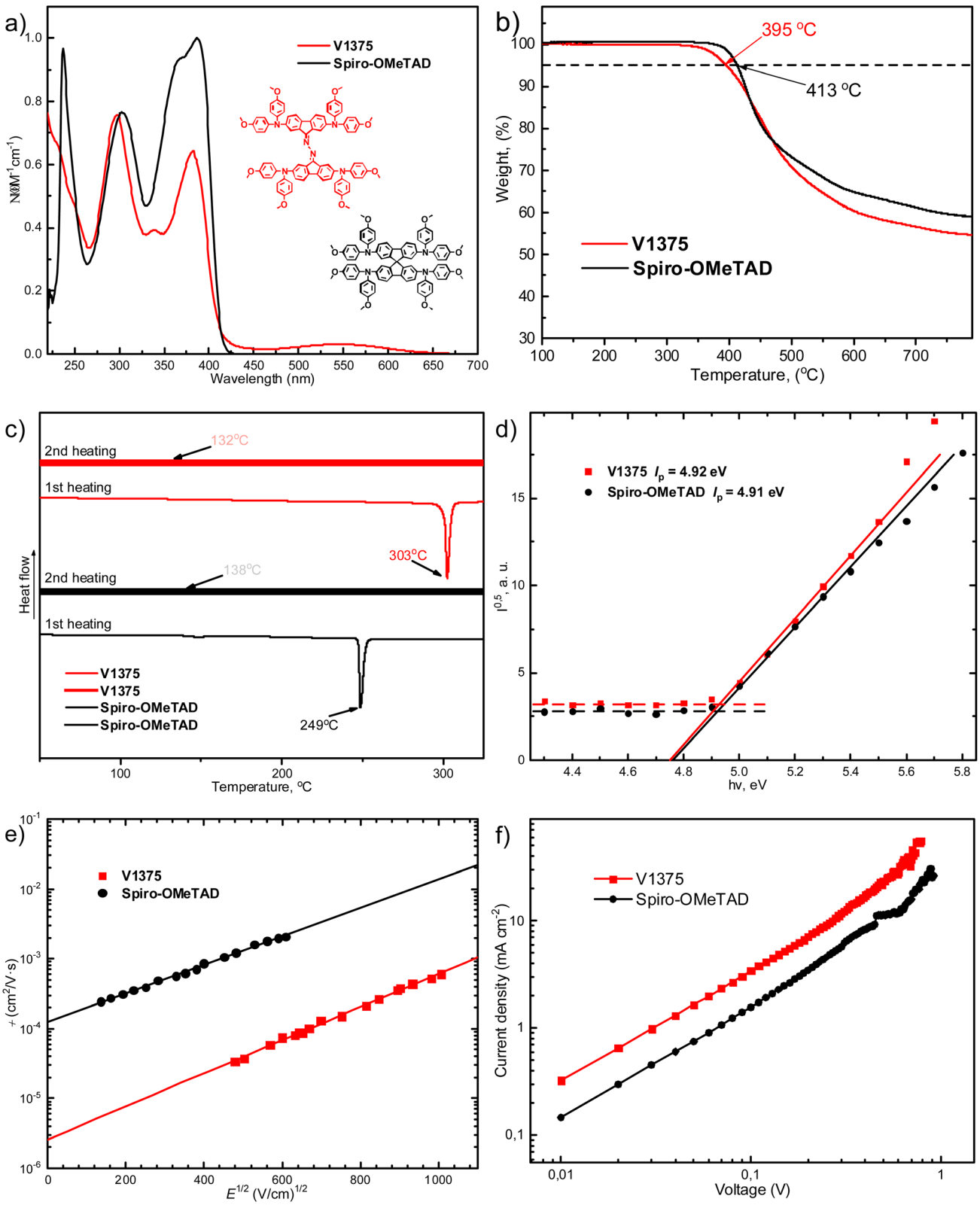

Fig. 3 (a) Normalized UV-vis absorption spectra of **V1375** and Spiro-OMeTAD from THF solution (10^{-4} M). (b) TGA heating curve of **V1375** and Spiro-OMeTAD (heating rate of 10 °C min^{-1}, N_2 atmosphere). (c) DSC curve of the first heating of **V1375** and Spiro-OMeTAD. (d) Ionization potential of **V1375** and Spiro-OMeTAD. (e) Hole drift mobility of target material **V1375** and Spiro-OMeTAD. (f) Conductivity of target material **V1375** and Spiro-OMeTAD.

was produced from 2,7-dibromofluoren-9-one *via* a hydrazone condensation reaction, yielding intermediate 1, which was filtered after the reaction, washed with hot acetone, and then treated with 4,4′-dimethoxydiphenylamine in the presence of a palladium catalyst to obtain the target material **V1375**. The chemical structure of the target material was confirmed by NMR spectroscopy and mass spectrometry. A detailed description of the synthetic procedures is provided in the (SI).

Considering the simple syntheses of **V1375**, its material costs were assessed based on the model described by Osedach, Andrew, and Bulovic,[33] which gives a figure of about 29.58 $ per g (Table S1). It would cost three times less to produce this HTM than the widely used standard Spiro-OMeTAD, which costs 92 $ per g to synthesize.

To determine the conjugation in the new compound, UV-vis absorption spectra in THF solution ($c = 10^{-4}$ M) were recorded (Fig. 3a). **V1375** exhibits four absorption peaks. The absorption spectrum of **V1375** is slightly redshifted compared to that of Spiro-OMeTAD, indicating negligible enhancement in π-conjugation. The peaks in the range of 230–425 nm can be assigned to π → π* transitions, whereas a barely noticeable absorption band in the visible region at 544 nm is a result of π → π* transitions with a charge transfer character, arising from the electron-rich hydrazone units. This is also in good agreement with the density functional theory (DFT) calculations, performed at the B3LYP/6-31G(d,p) level of theory, where the highest occupied molecular orbital (HOMO) of the **V1375** molecule is distributed mainly over the dimethoxy diphenylamine substituted fluorene fragments. Upon excitation, the lowest unoccupied molecular orbital (LUMO) is highly delocalized over the hydrazone units (Fig. 2).

The thermal properties of **V1375** were evaluated using thermogravimetric analysis (TGA) and differential scanning calorimetry (DSC). The results are presented in Table 1 and Fig. 3b, c. From the TGA data, it was found that hydrazone-based HTM demonstrates a relatively high decomposition temperature (T_{d5}) of 395 °C at 5% weight loss, which is similar to that of spiro-OMeTAD (413 °C), indicating the good thermal stability required for a photovoltaic device.[34] The DSC analysis revealed that **V1375** exhibited one endothermic peak, appearing at around 300 °C, which is typically associated with a melting process. No crystallization was observed during the cooling and second heating steps; only the glass transition (T_g) at 132 °C was observed, which is comparable to the T_g of Spiro-OMeTAD, suggesting that the material exists in both crystalline and amorphous states. Moreover, we evaluated the T_g of **V1375** upon mixing it with the additives that are typically employed in the fabrication of a PSC. As shown in Fig. S6, upon doping, **V1375** possesses a significantly lower T_g value compared to the undoped value (132 °C), which may be caused by the migration and volatilization of dopants at high temperatures.[35] We next evaluated the T_g of doped Spiro-OMeTAD, and it was found that upon doping, Spiro-OMeTAD suffers a significant drop in T_g, possessing an even lower T_g value of 67 °C compared to doped **V1375**; therefore, while the doped **V1375** T_g is 78 °C, it still demonstrates superior thermal stability at 65 °C *in operando* compared to the reference (Fig. S7).

The energy level of **V1375** was estimated by photoelectron spectroscopy in air (PESA), yielding an ionization potential (I_P) of 4.92 eV (see Table 1 and Fig. 3d). Compared with Spiro-OMeTAD (I_P = 4.91 eV), it is evident that the presence of a hydrazone group in the center of the molecule does not change the I_P, suggesting that the synthesized compound would be suitable for use in PSCs.

The hole drift mobility (μ_0) was measured using the xerographic time-of-flight (XTOF) method, and the results are presented in Table 1 and Fig. 3e. The data show that **V1375** exhibits a hole drift mobility of 2.5×10^{-6} cm^2 V^{-1} s^{-1} at zero electric field strength, which is lower than that of Spiro-OMeTAD ($\mu_0 = 1.4 \times 10^{-5}$ cm^2 V^{-1} s^{-1}). This difference can be attributed to the flexible backbone of the hydrazone-based material, which may induce conformational and energetic disorders, thereby reducing hole drift mobility. The intrinsic conductivity (σ) was evaluated using current measurement (Fig. 3f), and it was found that **V1375** has 2.5 times higher conductivity than Spiro-OMeTAD, at 1.6×10^{-4} and 6.4×10^{-5} S m^{-1}, respectively, attributed to the higher concentration of holes in the **V1375** material.

The performance of the constructed devices is summarized in Table 2. Fig. 4a and b present the *J–V* curves of the champion PSCs. The highest PCE of the reference (Spiro-OMeTAD) device was 23.97%, whereas the **V1375**-based device achieved 24.23%. The best-performing device of **V1375** exhibited a V_{OC} of 1.119 V, J_{SC} of 26.12 mA cm^{-2}, and a fill factor (FF) of 0.825. Additionally, the hysteresis indices (HI) were evaluated for both the reference and **V1375** devices (Fig. 4a and b), revealing that the latter exhibits lower HI values. The EQE spectra and statistics of the photovoltaic parameters are shown in Fig. S4 and S5.

The long-term stability of the PSCs was evaluated under maximum power point (MPP) tracking conditions for 950 hours in an inert environment (Fig. 4c). After this period, the reference device retained only 65% of its initial efficiency, whereas devices employing **V1375** as the HTM exhibited improved stability, maintaining 85% of their original efficiency. Additional MPP decay measurements were conducted at 65 °C. All PSCs were tested in an N_2 atmosphere under continuous illumination of 100 mW cm^{-2}. As shown in Fig. 4d, the device incorporating **V1375** as the HTM exhibited superior thermal stability compared to the untreated reference device. After 500 hours of continuous light soaking, the **V1375**-based device retained 89% of its initial MPP value, whereas the reference devices maintained only 75%.

Table 2 PV characteristics derived from the corresponding *J–V* curves of the best-performing devices

HTM	V_{oc} [V]	J_{sc} [mA cm^{-2}]	FF	PCE [%]
V1375	1.119	26.12	0.825	24.23
Spiro-OMeTAD	1.113	26.09	0.822	23.97

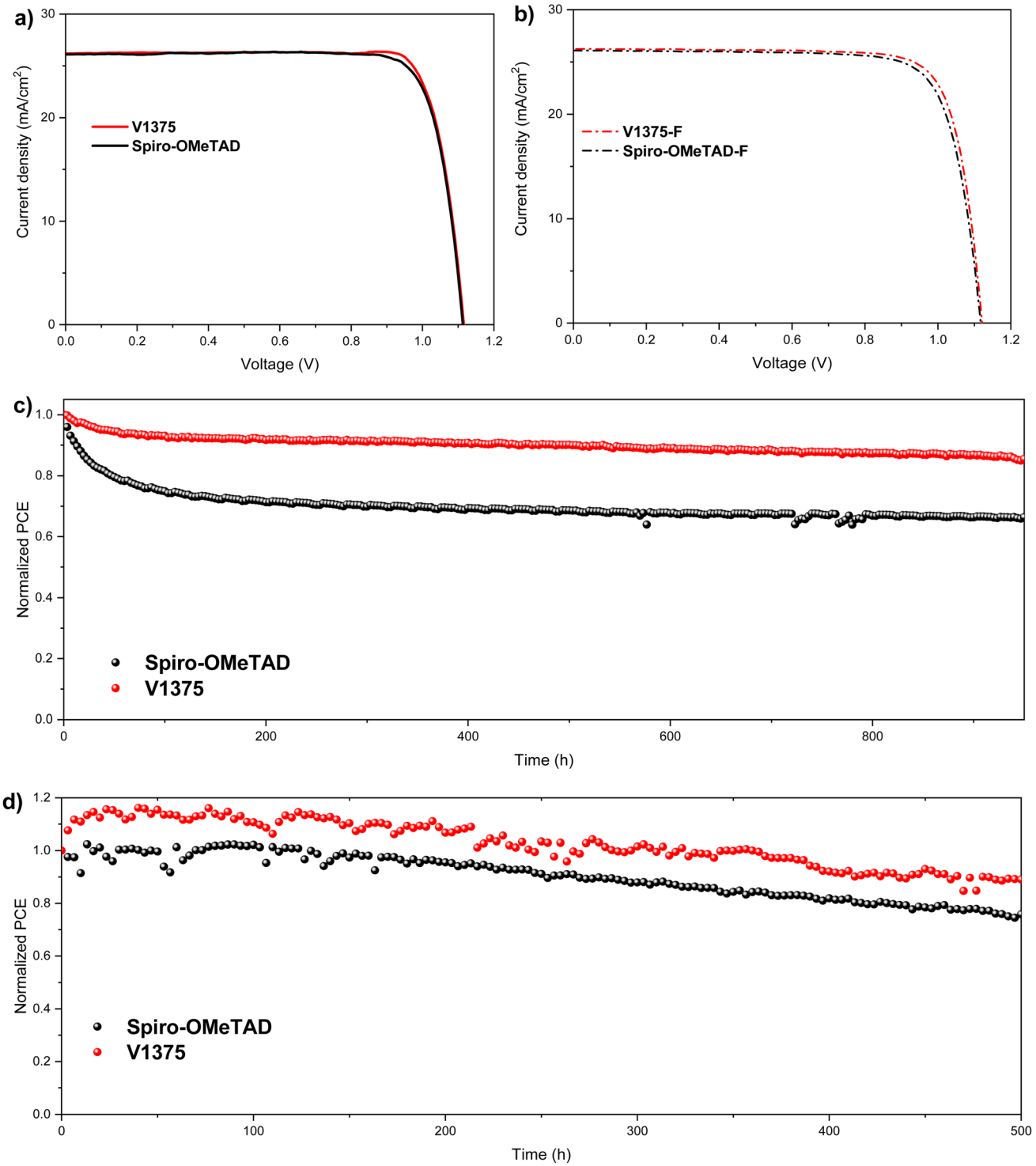

Fig. 4 (a) *J*–*V* reverse scan (RS) curves and (b) *J*–*V* forward scan (FS) curves of the perovskite champion devices with **V1375** and reference devices recorded under one sun illumination. (c) Light-induced stability of perovskite devices incorporating **V1375** and reference materials. The devices were measured in an N_2 atmosphere at room temperature, under constant illumination (LED source, ≈1 Sun) at the maximum power point for 950 h. (d) Thermal stability of perovskite devices incorporating **V1375** and reference materials. The devices were measured in an N_2 atmosphere at 65 °C, under continuous illumination (LED source, ≈1 Sun) at a maximum power point for 500 h.

Conclusion

In this study, a hydrazone-based HTM, **V1375**, containing 4,4′-dimethoxydiphenylamine chromophores, was synthesized and evaluated as a potential replacement for Spiro-OMeTAD in perovskite solar cells. **V1375** exhibits high thermal stability and a relatively high glass transition temperature. Perovskite solar cells incorporating **V1375** achieved a maximum efficiency of

24.23%, outperforming the benchmark Spiro-OMeTAD (23.97%). The simplicity of a cost-effective and upscalable synthesis should enable the rapid advancement of this material for perovskite solar cells and other optoelectronic applications.

Author contributions

A. J. and P. L. performed the synthesis and wrote the first manuscript draft. X.-X. G. designed the experiments and fabricated the PSCs. M. D. and J. P. contributed to DFT calculations and molecular dynamics simulations. S. X. and R. P. helped with the device fabrication and characterization. V. J. performed hole mobility measurements. K. R. was involved in discussion and project coordination. M. K. N. and V. G. supervised the project. All the authors contributed to the revisions.

Conflicts of interest

There are no conflicts to declare.

Data availability

The data that supports the findings of this study are available within the article and its supplementary information (SI). Additional data will be available online under a repository link once the article has been accepted for publication, or from the corresponding author upon request. Supplementary information is available. See DOI: https://doi.org/10.1039/d5ta10419j.

Acknowledgements

This project is co-funded by the European Union. Views and opinions expressed are, however, those of the author(s) only and do not necessarily reflect those of the European Union or the European Climate, Infrastructure and Environment Executive Agency (CINEA). Neither the European Union nor the granting authority can be held responsible for them. PEPPERONI, ID: 101084251. We acknowledge the funding from the project "Mission-driven Implementation of Science and Innovation Programmes" (No. 02-002-P-0001), funded by the Economic Revitalization and Resilience Enhancement Plan "New Generation Lithuania".

References

1 D. M. Chapin, C. S. Fuller and G. L. Pearson, *J. Appl. Phys.*, 1954, **25**(5), 676–677.
2 A. Kojima, K. Teshima, Y. Shirai and T. Miyasaka, *J. Am. Chem. Soc.*, 2009, **131**(17), 6050–6051.
3 https://www.nrel.gov/pv/cell-efficiency.html, (accessed: October 2025).
4 Q. Dong, Y. Fang, Y. Shao, P. Mulligan, J. Qiu, L. Cao and J. Huang, *Science*, 2014, **347**(6225), 967–970.
5 W. J. Yin, T. Shi and Y. Yan, *Adv. Mater.*, 2014, **26**, 4653–4658.
6 A. Miyata, A. Mitioglu, P. Plochocka, O. Portugall, J. T. W. Wang, S. D. Stranks, H. J. Snaith and R. J. Nicholas, *Nat. Phys.*, 2015, **11**, 582–587.
7 C. Wehrenfennig, G. E. Eperon, M. B. Johnston, H. J. Snaith and L. M. Herz, *Adv. Mater.*, 2014, **26**, 1584–1589.
8 N. K. Elangovan, R. Kannadasan, B. B. Beenarani, M. H. Alsharif, M. K. Kim and Z. H. Inamul, *Energy Rep.*, 2024, **11**, 1171–1190.
9 H. Miah, B. Rahman, M. Nur-E-Alam, M. A. Islam, M. Shahinuzzaman, R. Rahman, H. Ullahi and M. Khandaker, *RSC Adv.*, 2025, **15**, 628–654.
10 R. R. Sova, Shobih, W. Budiawan, W. Septina, L. Yuliantini, Y. Firdaus, E. Almuqoddas, B. Yuliarto and N. M. Nursam, *Synth. Met.*, 2024, **306**, 117646.
11 W. Passatorntaschakorn, W. Khampa, W. Musikpan, A. Ngamjarurojana, A. Gardchareon, P. Kanjanaboos, A. Kaewprajak, P. Kumnorkaew, P. Ruankham and D. Wongratanaphisan, *ACS Appl. Energy Mater.*, 2024, **7**(16), 6972–6985.
12 G. Huang, T. Zhang, W. Lin, L. Qin, S. Z. Kang and X. Li, *Angew. Chem., Int. Ed.*, 2025, **64**, e202420687.
13 S. Mattiello, G. Lucarelli, A. Calascibetta, L. Polastri, E. Ghiglietti, S. K. Podapangi, T. M. Brown, M. Sassi and L. Beverina, *ACS Sustainable Chem. Eng.*, 2022, **10**(14), 4750–4757.
14 Y. Ren, Y. Wei, T. Li, Y. Mu, M. Zhang, Y. Yuan, J. Zhanga and P. Wang, *Energy Environ. Sci.*, 2023, **16**, 3534–3542.
15 X. Wang, M. Wang, Z. Zhang, D. Wei, S. Cai, Y. Li, R. Zhang, L. Zhang, R. Zhang, C. Zhu, X. Huang, F. Gao, P. Gao, Y. Wang and W. Huang, *Research*, 2024, **7**, 0332.
16 Y. Luo, T. Li, L. He, L. Dong, T. Xie, Y. Ren, Z. Zhang, G. Yang, Y. Jia, J. Zhou and K. Guo, *Adv. Funct. Mater.*, 2025, **35**, 2419849.
17 R. Li, M. Liu, S. K. Matta, A. Almasri, J. Tian, H. Wang, H. P. Pasanen, S. P. Russo, P. Vivo and H. Zhang, *Sol. RRL*, 2023, **7**, 2300367.
18 P. Mäkinen, F. Fasulo, M. Liu, G. K. Grandhi, D. Conelli, B. Al-Anesi, H. Ali-Löytty, K. Lahtonen, S. Toikkonen, G. P. Suranna, A. B. Muñoz-García, M. Pavone and R. Grisorio, *Chem. Mater.*, 2023, **35**(7), 2975–2987.
19 C. Hao, X. Zong, Y. Cheng, M. Zhao, M. Luo, Y. Zhanga and S. Xue, *Sustain. Energy Fuels*, 2021, **5**, 5548–5556.
20 A. Jegorovė, J. Xia, M. Steponaitis, M. Daskeviciene, V. Jankauskas, A. Gruodis, E. Kamarauskas, T. Malinauskas, K. Rakstys, K. A. Alamry, V. Getautis and M. K. Nazeeruddin, *Chem. Mater.*, 2023, **35**(15), 5914–5923.
21 B. Xiao, Y. Yang, S. Chen, Y. Zou, X. Chen, K. Liu, N. Wang, Y. Qiao and X. Yin, *Sol. RRL*, 2022, **6**, 2100990.
22 S. C. Lin, T. H. Cheng, C. P. Chen and Y. C. Chen, *Mater. Chem. Phys.*, 2022, **288**, 126385.
23 A. A. Sutanto, V. Joseph, C. Igci, O. A. Syzgantseva, M. A. Syzgantseva, V. Jankauskas, K. Rakstys, V. I. E. Queloz, P. Y. Huang, J. S. Ni, S. Kinge, A. M. Asiri, M. C. Chen and M. K. Nazeeruddin, *Chem. Mater.*, 2021, **33**(9), 3286–3296.
24 H. Liu, B. He, H. Lu, R. Tang, F. Wu, C. Zhong, S. Li, J. Wang and L. Zhu, *Sustain. Energy Fuels*, 2022, **6**, 371–376.
25 Y. J. Kim, B. Yang, J. Suo, E. Jatautiene, J. Simokaitiene, R. Durgaryan, D. Volyniuk, A. Hagfeldt, G. Sini and J. V. Grazulevicius, *Nano Energy*, 2022, **101**, 107618.

26 J. Simokaitiene, A. Danilevicius, S. Grigalevicius, J. V. Grazulevicius, V. Getautis and V. Jankauskas, *Synth. Met.*, 2006, **156**(14–15), 926–931.
27 R. Budreckiene, J. V. Grazulevicius, V. Jankauskas, J. Vedegyte and J. Sidaravicius, *J. Optoelectron. Adv. Mater.*, 2006, **8**(4), 1533–1537.
28 R. Budreckiene, V. Andruleviciute, G. Buika, J. V. Grazulevicius, V. Jankauskas and V. Grazuleviciene, *Mater. Sci. Pol.*, 2009, **27**(1), 61–72.
29 M. L. Petrus, M. T. Sirtl, A. C. Closs, T. Bein and P. Docampo, *Mol. Syst. Des. Eng.*, 2018, **3**, 734–740.
30 M. L. Petrus, A. Music, A. C. Closs, J. C. Bijleveld, M. T. Sirtl, Y. Hu, T. J. Dingemans, T. Bein and P. Docampo, *J. Mater. Chem. A*, 2017, **5**, 25200–25210.
31 C. Decavoli, C. L. Boldrini, A. Abbotto and N. Manfredi, *Eur. J. Org Chem.*, 2023, **26**, e202201511.
32 R. Durgaryan, J. Simokaitiene, A. Dabuliene, D. Volyniuk, O. Bezvikonnyi, V. Jankauskas, V. Matulis, D. Lyakhov, I. Klymenko, B. Schmaltz and J. V. Grazulevicius, *Synth. Met.*, 2022, **287**, 117057.
33 T. P. Osedach, T. L. Andrew and V. Bulovic, *Energy Environ. Sci.*, 2013, **6**, 711–718.
34 R. Gehlhaar, T. Merckx, W. Qiu and T. Aernouts, *Glob. Chall.*, 2018, **2**, 1800008.
35 X. Wang, Y. Zhong, Y. Liu, X. Luo, B. Gao, L. Tan and Y. Chen, *Angew. Chem., Int. Ed.*, 2025, **64**, e202424191.

